Simulation Modelling Practice and Theory 41 (2014) 87–103

Contents lists available at ScienceDirect

Simulation Modelling Practice and Theory

journal homepage: www.elsevier.com/locate/simpat

# On the machining induced residual stresses in IN718 nickel-based alloy: Experiments and predictions with finite element simulation

P.J. Arrazola [a], A. Kortabarria [a], A. Madariaga [a], J.A. Esnaola [a], E. Fernandez [a], C. Cappellini [b], D. Ulutan [c], T. Özel [c,*]

[a] Faculty of Engineering, Mondragon University, Arrasate-Mondragón, Spain
[b] Department of Industrial & Mechanical Engineering, University of Brescia, Brescia, Italy
[c] Department of Industrial & Systems Engineering, Rutgers University, Piscataway, NJ, USA

ARTICLE INFO

*Article history:*
Received 4 June 2012
Received in revised form 24 September 2013
Accepted 18 November 2013
Available online 15 December 2013

*Keywords:*
Residual stress
X-ray diffraction
Finite element simulation

ABSTRACT

Residual stresses after machining processes on nickel-based super alloys is of great interest to industry in controlling surface integrity of the manufactured critical structural components. Therefore, this work is concerned with machining induced residual stresses and predictions with 3-D Finite Element (FE) based simulations for nickel-based alloy IN718. The main methods of measuring residual stresses including diffraction techniques have been reviewed. The prediction of machining induced stresses using 3-D FE simulations and comparison of experimentally measured residual stresses for machining of IN718 have been investigated. The influence of material flow stress and friction parameters employed in FE simulations on the machining induced stress predictions have been also explored. The results indicate that the stress predictions have significant variations with respect to the FE simulation model and these variations can be captured and the resultant surface integrity can be better represented in an interval. Therefore, predicted residual stresses at each depth location are given in an interval with an average and standard deviation.



## 1. Introduction

Nickel-based super alloys are commonly used for mission critical structural components in hot sections of aircraft engines and gas turbines. Their high mechanical strengths at both low and high temperatures and corrosion resistance properties make these alloys highly suitable for such applications. During manufacturing of these components, machining processes are often utilized as the final process. Machining processes may induce mechanical (plastic deformations, hardness profile, residual stresses), metallurgical (phase transformation, precipitation, recrystallization), chemical, and thermal (heat-affected layer) alterations to the surface and subsurface of these components. As a result, machining induced mechanical surface integrity that includes surface roughness, residual stresses and subsurface plastic deformations plays an important role in the fatigue life of these mission critical structural components. Among Ni-based super alloys, Inconel 718 (IN718) which is a Nickel–Fe–Cr alloyed material is extensively used in aircraft components such as turbine disks and shafts.

There exist extensive reviews about machining induced surface integrity on metal alloys including titanium and nickel based alloys [14,17,4]. It is widely reported that during machining of IN718 nickel-based alloy, plastic deformations from chip formation, mechanical tool forces, friction between tool-workpiece, and heat generation result in severe thermal and

* Corresponding author. Tel.: +1 732 445 1099.
*E-mail address:* ozel@rutgers.edu (T. Özel).

1569-190X/$ - see front matter © 2013 Elsevier B.V. All rights reserved.
http://dx.doi.org/10.1016/j.simpat.2013.11.009

mechanical strains and stresses on the machined surface especially beneath the tool edge area along the tool flank face. Combined thermal strain and plastic deformations leave significant residual stresses on the surface and into the depth of material after the machining process. While these stresses can be removed through post-processing by using stress relief methods, it is more economical to design machining processes properly and select optimum cutting tool material and geometry, and cutting conditions that can provide the most desirable surface integrity in these mission critical structural components.

Finite Element (FE) based simulations have the potential to provide a platform to design the machining process and virtually test the cutting tool material and geometry selected in various cutting conditions. In response to input variables, FE simulations can produce very rich set of output data such as predicted tool forces, strain, stress and temperature fields [10].

However, FE simulation results highly depend on the workpiece material constitutive model (or flow stress data), representing the friction conditions between tool and workpiece (or chip), physical and thermal properties of tool and work material as well as simulation settings (i.e. mesh topography, density and element size, time increment size, remeshing strategies, relative force and velocity error tolerance). While FE simulation of machining processes still presents significant challenges it is a great interest for the manufacturing industry. Therefore, this paper focuses on experimental and 3-D FE-based simulation investigations on machining induced residual stresses in IN718 nickel-based super alloy and compares the simulation predictions with experiments in order to reveal the effectiveness and accuracy of 3-D FE simulations.

In this study, a new set of face turning experiments has been conducted on a precipitation hardened IN718 nickel-based alloy in order to compare the experimental results with forces and stresses predicted from 3-D FE simulations. At the same cutting conditions, residual stress profiles have been measured by the using X-ray diffraction technique and utilized in comparison of machining induced stress profiles obtained from 3-D FE simulations.

## 2. Machining induced residual stress

Following machining processes, residual stresses, which remain in the material after unloading, are often tensile on the surface due to thermal strains and turn compressive due to plastic deformations in the subsurface of the work material and possess potential risks in fatigue failure. Machining induced stresses during turning process can induce stress in cutting or circumferential (hoop) direction and in longitudinal (depth) or axial direction as shown in Fig. 1. It is often required to ameliorate tensile surface residual stresses into compressive stresses by post-processing techniques such as shot peening and burnishing or prevent them from occurring during machining processes. A review of research studies on the effects of machining parameters reveal that it is generally observed that by increasing cutting speed, tensile residual stresses tend to become more compressive due to greater plastic deformations, while increases in depth of cut and feed rate have some effect on making the residual stresses more tensile at the surface and more compressive in the peak compressive depth [17]. In order to fully understand machining induced residual stresses, a critical review and discussion on residual stress measurement techniques is needed. For this reason, a brief review of such measurement techniques is given with their distinct advantages and disadvantages in this paper.

### *2.1. Residual stress measurement techniques*

#### *2.1.1. Destructive techniques*

Some of the methods to measure residual stresses are destructive, which means that during the measurement, the workpiece material is physically damaged. The most commonly used destructive methods are sectioning and hole drilling. In sectioning method, after each measurement, a layer of the material is removed by a predefined removal process, and then the next measurement can be taken. Usually, the distance between measurements is in the order of 1 mm or 100 μm [19,2,5].

In the hole drilling method, a blind hole (conventionally between 1 or 2 mm in diameter depending on gauge size) is drilled into the workpiece before taking any measurements, and along that hole, measurements are taken, with 100 μm

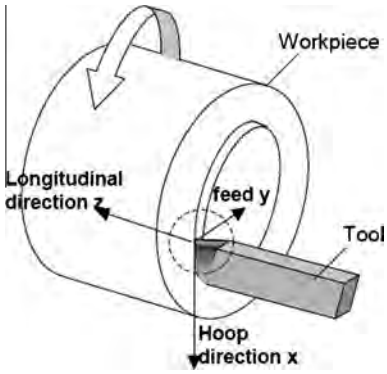


**Fig. 1.** Machining induced stresses in cutting or circumferential (hoop) direction and in axial (longitudinal) or depth direction in face turning processes [6].

to 1 mm distances from one another, with the help of a strain gauge rosette glued to the hole at the surface of the material [19]. The strain gauge position within the blind hole measures the relaxation of the strain and the residual stresses are calculated from these strain values [2]. The minimum depth of measurement is usually half the diameter of the drilled hole, which is the main constraint with this method. Hence, the accuracy of the distances between measurements is more than tens of micrometers in these destructive methods, and it is not suitable to obtain accurate readings from the first 100 μm.

#### 2.1.2. Non-destructive techniques

There are also several methods that are non-destructive, which are qualitative rather than quantitative, which means that their results would only be informative about the whereabouts of the actual residual stress value, rather than giving specific value results [2]. Diffraction methods (neutron and X-ray diffraction) are found to be optimal for residual stress measurements in terms of accuracy, cost, speed, repeatability, and compatibility [2]. The penetration of the beam within the material and their diffracted angles give the quantitative information about the strain within the material, making the inter-atomic spacing in the material act like a strain gauge. In neutron diffraction, neutrons are used to diffract and detect, which limits the method to proximity of a nuclear reactor for the production of neutrons, also making the method very expensive [19]. Since these diffraction methods use the crystalline property of the materials to diffract a beam, they are only applicable to crystalline, polycrystalline, and semi-crystalline materials [2]. The penetration of the neutrons within the material and their diffracted angles give the quantitative information about residual stresses without causing permanent damage to the material. On the other hand, in X-ray diffraction (XRD), an X-ray beam is used to diffract and detect, which is comparably easier to produce. X-ray diffraction was found to be the optimal measuring technique when quantitative and accurate results are needed. Despite its higher cost, it is widely favored over hole drilling method due to its non-destructive nature and capability of measuring significantly closer to the surface [5].

#### 2.1.3. Comparison of residual stress measurement methods

In an experimental study, Ruud et al. [13] compared three main residual stress measurement methods; (i) blind hole drilling (SRT), (ii) X-ray diffraction, and (iii) Barkhausen Noise Analysis (BNA). Their XRD results showed tensile residual stresses on the surface with an inhomogeneous stress field and extraordinarily large grain size. The SRT results were in good agreement with XRD results when the depth levels were similar. The capability of BNA was far away from the surface, which made it harder to compare to XRD results, but it was significantly different than SRT results as well. The qualitative results were in agreement, but BNA lacked quantitative comparison due to the absence of a zero-stress standard for the BNA method.

Walker [19] investigated the methods of residual stress measurement without going into numerical details of experimental results and reported that X-ray diffraction method measures the residual stresses closest to the surface ($\sim$8 μm). Lord et al. [7] compared the accuracies of XRD and hole drilling methods. They reported that with the hole drilling method, the quantitative results of residual stresses were similar to the XRD results, but the measurements were made between $\sim$125 μm and 1.25 mm. Their results indicate that XRD and hole drilling results match qualitatively and quantitatively through the whole material. Benediktovich et al. [3] investigated the effect of surface roughness on residual stress measurements using the XRD method. They claimed that with changing surface roughness, the refractive properties of the studied area change, causing variability in the measurements. Belassel et al. [2] compared many different techniques of residual stress measurement such as XRD, neutron diffraction, hole drilling, sectioning, BNA, Eddy current, and ultrasonic methods. It was stated that hole drilling method was not capable of measuring surface or immediate subsurface residual stresses and the regions covered with SRT and XRD methods are different. In summary, researchers agreed that it is essential to decide on the needed method to measure the residual stresses according to the requirements of the process, and obtain measurements qualitatively rather than quantitatively, as there is often significant amount of uncertainty in the measurements.

### 2.2. Machining induced residual stresses in nickel alloys

The work on experimenting and measuring residual stress induced by machining processes have been reviewed by several review papers in recent years [14,17,4]. It has been concluded that many researchers have utilized the X-ray diffraction technique for the measurement of residual stresses induced by machining, and especially for titanium and nickel-based alloys, this method is the most commonly used one. Among these, Arunachalam et al. [1] in their research work analyzed the effect of insert shape and coolant in the machining induced near surface residual stresses in IN718 nickel based alloy. The conclusions of this study which is particularly important to this work are summarized in Table 1.

In a study on the effects of tool coating on machining-induced residual stresses on both hoop (cutting speed) and radial (feed) directions in the nickel-based alloy IN718 [9], it was found that addition of coating material increases the tensile surface residual stresses, but pushes the compressive residual stress peak value to deeper into the material (Fig. 2).

Li et al. [6] utilized a powder metallurgy route nickel-based superalloy, RR1000, in order to study the residual stresses within face turned material. They used the XRD technique in measuring the residual stresses on the disk, and observed the variations in the measurements with changing radial location on the disk through the depth of the material. They found that the radial direction residual stresses are less tensile on the surface compared to the hoop direction residual stresses, and claimed that the inner diameter and outer diameter measurements for the radial direction residual stresses were very similar to each other (Fig. 3). However, their results show that the residual stress measurement in the hoop direction vary between the inner and the outer diameter.

**Table 1**
The effect of tool shape and coolant in surface residual stresses in machining IN718. [1].

| Tool parameter | Effect on surface roughness | Effect on residual stresses |
|---|---|---|
| Insert shape (round or square) | Use of round inserts results in lower values | Use of round inserts results in compressive residual stresses |
| Cutting edge preparation (sharp, honed, chamfered) | Increasing order of surface roughness: honed, chamfered, sharp | Decreasing order of compressive residual stresses: chamfered, honed, sharp |
| Insert rake type (positive or negative) | Positive rake inserts produce lower values when coolant is used and results in higher values in dry cutting | Negative rake inserts produce compressive stresses while positive rake inserts give tensile residual stresses |
| Nose radius (0.8, 1.2 and 1.6 mm) | Increasing order of surface roughness: 1.6, 1.2, 0.8 mm | Decreasing order of compressive residual stresses: 0.8, 1.6, 1.2 mm |
| Effect of coolant | Use of coolant results in lower values | Use of coolant results either in compressive stresses or lower values of tensile residual stresses |

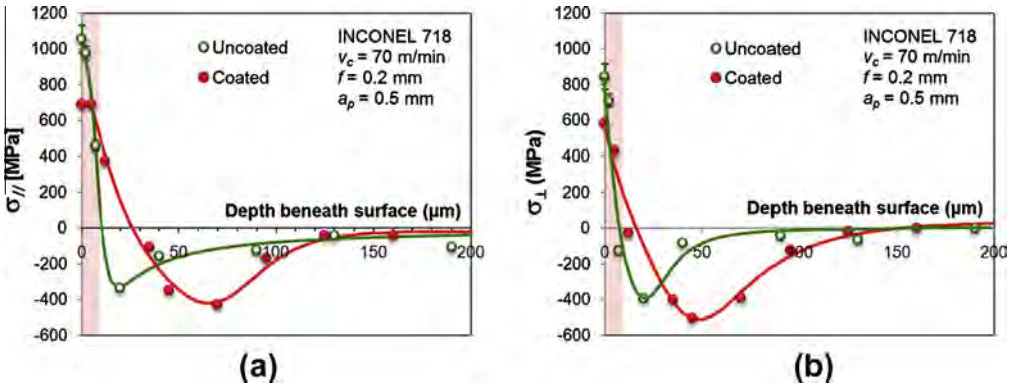


**Fig. 2.** Residual stress profile of IN718 in (a) cutting direction and (b) in feed direction after turning at $v_c = 70\ \mathrm{m \cdot min^{-1}}$, $f = 0.2$ mm, and $a_p = 0.5$ mm [9].

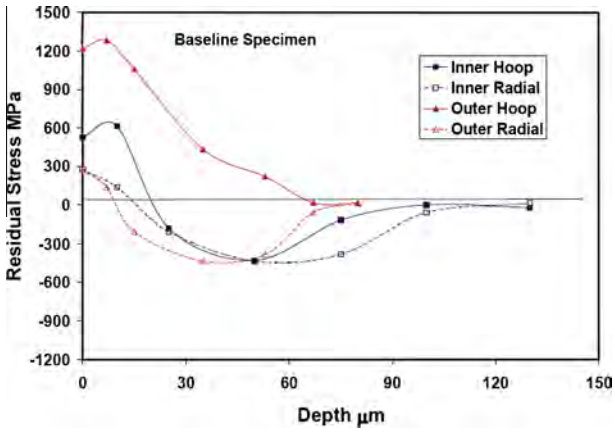


**Fig. 3.** Inner and outer diameter measurements for hoop and radial direction residual stresses [6].

In another study [5], researchers tried to compare two of the most common techniques in residual stress measurements, hole drilling and XRD, and compare their FEM-based simulation findings with both measurements (Fig. 4). Their results show that XRD has the capability to gather measurements at the surface of the material, whereas hole drilling method lacks this capability. The accuracy of the two methods is debatable, and since there is no completely proven and robust method of measuring residual stress at near-surface at the moment, the results from both methods seem to be consistent with expectations. Although there are many studies reported about machining induced residual stress measurements in the literature, very few of them are actually related to nickel-based alloys. Furthermore, as pointed out by Jawahir et al. [4] large differences exist in simulation studies on machining induced residual stresses in IN718 nickel based alloy, therefore further research on material model parameter effects on residual stress predictions in machining of this alloy material was recommended.

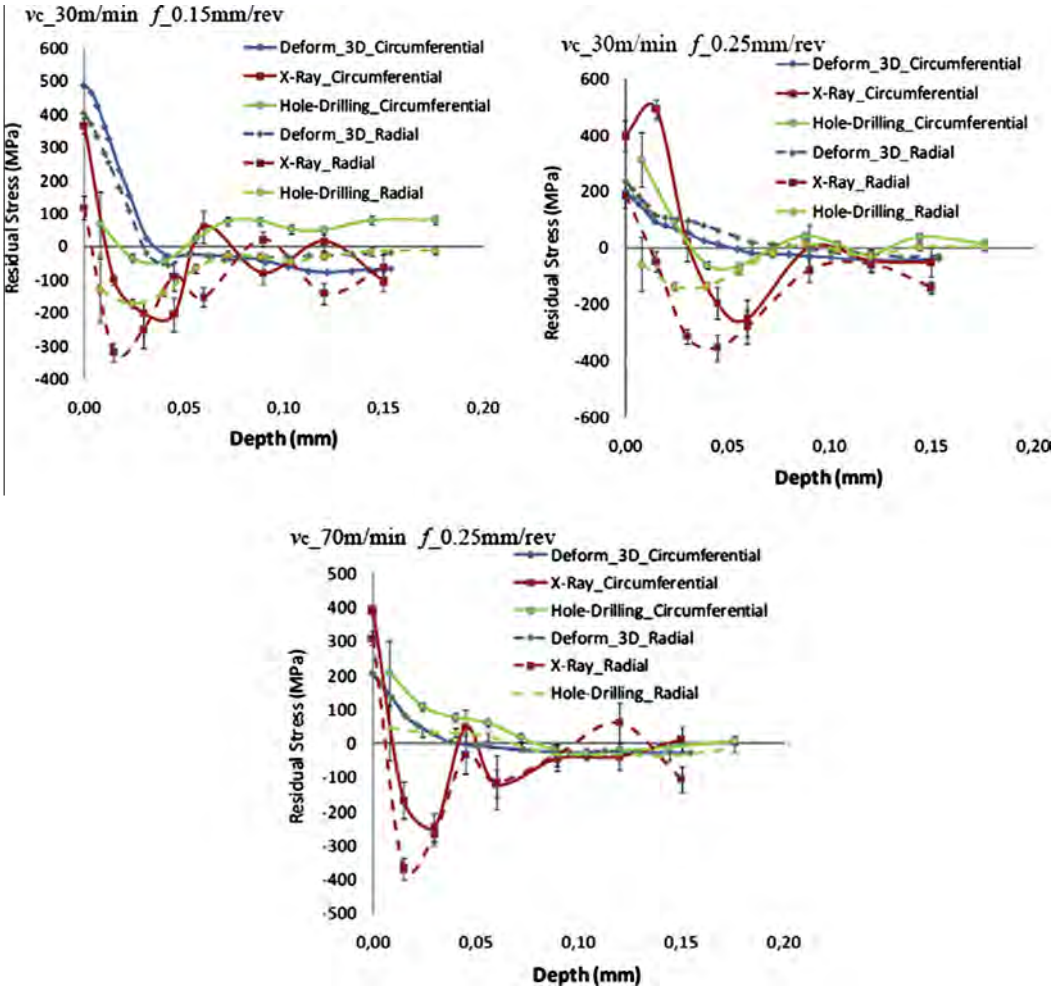


**Fig. 4.** Comparison of residual stress measurements with XRD and hole drilling, and numerical findings from FE-based model in circumferential and radial directions after face turning IN718 [5].

Özel and Ulutan [11] investigated machining induced residual stresses experimentally through-the-thickness in face turning of IN-100 workpiece material which is a Ni–Co–Cr based nickel alloy by using a triangular type (insert nose radius of 0.8 mm) uncoated and TiAlN carbide insert (edge radius of 10–25 μm) at a cutting speed ($v_c$) of 24 m min$^{-1}$, a feed ($f$) of 0.05 mm rev$^{-1}$ and a depth of cut ($a_p$) of 1.0 mm. They concluded that residual stresses become more compressive with increased edge radius but more tensile at the surface when the tool is coated with TiAlN.

## 3. Experimental work

In this study, face turning experiments have been designed and conducted in order to measure cutting forces during machining and residual stresses on the surface of the IN718 nickel-based alloy material after machining by using the XRD method. The work specimen was a 50 mm diameter round bar of IN718 nickel-based alloy which was heat treated at 955 °C and subsequently quenched for one hour, that provided a hardness value of 45HRC.

### 3.1. Experimental setup

At the first phase of the experiments, disk shaped specimens of 50 mm in diameter and 15 mm in thickness have been sliced from a bar stock by using the Wire Electrical Discharge Machining (EDM) process. Before performing the actual machining tests, a facing operation has been carried out in a Computer Numerical Controlled (CNC) lathe as shown in Fig. 5 in order to ensure the same initial surface conditions in all specimens by employing a cutting speed ($v_c$) of 40 m min$^{-1}$, a feed ($f$) of 0.25 mm rev$^{-1}$ and a depth of cut ($a_p$) of 0.25 mm using conventional cooling.

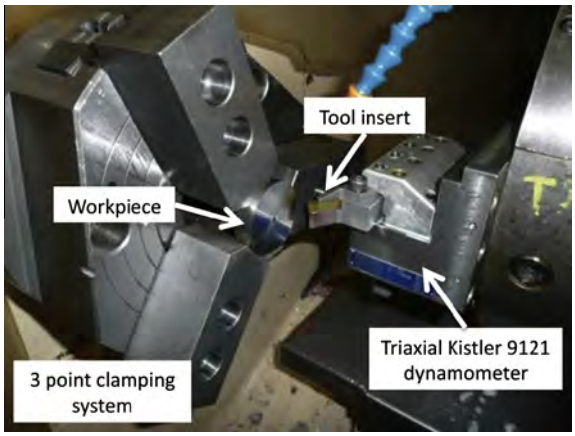


**Fig. 5.** Workpiece specimen and tool insert position in the CNC lathe during the testing.

After this phase, facing tests were carried out at different cutting speeds ($v_c$ = 30 and 70 m min$^{-1}$) and at different feeds ($f$ = 0.15 and 0.25 mm rev$^{-1}$) by employing coolant in the same CNC lathe. This lathe is capable of machining round workpieces up to 100 mm in diameter with a maximum constant cutting speed of $v_c$ = 30 m min$^{-1}$ and up to 250 mm in diameter with a maximum constant cutting speed of $v_c$ = 70 m min$^{-1}$. For each cutting test, a fresh cemented tungsten carbide tool insert was employed. Tool geometry and cutting conditions used in the experiments are summarized in Table 2. Forces in cutting (circumferential), $F_c$, feed (radial), $F_f$, and axial (depth), $F_p$, directions have been measured by using a triaxial Kistler 9121 dynamometer (see Fig. 5).

### 3.2. Residual stress measurements

The XRD method has been selected to measure residual stress profiles induced by face turning. As the XRD technique only allows measuring residual stresses on the surface, material layers have been removed by an electro-polishing process in order to determine residual stress profiles along the depth into the material. As it is shown in Fig. 6, residual stresses have been measured at least three times in each specimen at a distance of 18 mm from the center of the specimen. Residual stresses were determined in hoop (circumferential) direction (parallel to the cutting direction) and in the radial direction (parallel to the feed direction).

**Table 2**
Tool geometry and cutting parameters used in experimental testing and in the FE simulations.

| | |
|---|---|
| Insert radius, $r_\varepsilon$ (mm) | 4 |
| Insert edge radius, $r_\beta$ (μm) | 40 ± 5 |
| Clearance angle $\gamma_n$ (°) | 7° |
| Rake angle $\alpha_0$ (°) | 0° |
| Cutting speed, $v_c$ (m min$^{-1}$) | 30; 70 |
| Feed, $f$ (mm rev$^{-1}$) | 0.15; 0.25 |
| Depth of cut, $a_p$ (mm) | 0.15 |

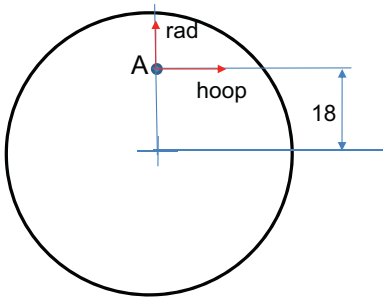


**Fig. 6.** Measurements of residual stress profiles by X-ray diffraction method.

Residual stresses on IN718 disks were measured using the XRD technique with the $\sin^2\psi$ method on a Proto iXRD diffractometer unit with Mn K$\alpha$ radiation at a diffraction angle of 151° to acquire diffraction peaks on the plane {3 1 1} at an irradiated area of 2 mm diameter spot. In order to obtain the maximum accuracy, measurements were performed at 9 diffraction angles with a time exposure of 60 s each.

These measured residual stress profiles have been reported together with force measurements and finite element simulation predictions in the following sections.

## 4. Finite element simulations

Finite element-based simulations for face turning of thin IN718 nickel-based alloy are designed using 3-D modeling to investigate the machining induced stress profiles and compare with experimentally measured residual stresses.

In 3-D modeling of machining, an updated incremental Lagrangian formulation, DEFORM-3D™, finite element software specialized for modeling of machining operations has been employed similar to the work by Özel et al. [10] and Özel and Ulutan [11]. The software allows a coupled modeling of deformation and heat transfer using implicit integration method and by using automatic remeshing techniques, elastic–viscoplastic material flow around the cutting tool tip can be simulated. For this purpose, a finite element model as shown in Fig. 7 has been created. In this model, the DEFORM-3D FE software provides a coupled solution for the mechanical elastic–viscoplastic deformations and heat transfer analysis by computing heat generated from deformations and frictional contact between the tool and the workpiece.

DEFORM-3D uses an incremental updated Lagrangian displacement field solution for computing large plastic deformations that are caused by an external global load vector (cutting tool advance) through transferring deformable body (workpiece) into resultant displacements that are subjected to a stiffness matrix. In the meshed model of the workpiece, an elastic–viscoplastic deformable body was represented with 70,000 (in average) elements. A cemented tungsten carbide (P10 grade) round insert ($r_\varepsilon$ = 4 mm radius) and with a cutting edge radius of $r_\beta$ = 40 μm was modeled as rigid body represented with 50,000 (in average) elements. Four-node tetrahedral finite elements with minimum element size between 5 and 10 μm (in average), a maximum element size between 200 and 300 μm (in average) with a size ratio of 30 are used. In the vicinity of the tool and workpiece contact, a very fine mesh is employed to simulate the chip formation process during machining (see Fig. 7). The tool geometry and tool holder angles and process conditions employed in experimental tests that were also used in FE simulations are shown in Table 2.

Thermal boundary conditions are defined accordingly in order to allow heat transfer from workpiece to the cutting tool. The heat conduction coefficient ($h$) is taken as $10^5$ W m$^{-2}$ K$^{-1}$ to allow rapid temperature rise in the tool. Mechanical and thermo-physical properties of IN718 nickel-based alloy are defined as temperature-dependent ($T$ in °C). Particularly, temperature-dependent modulus of elasticity ($E$ in MPa), thermal expansion ($\alpha$ in mm mm$^{-1}$ °C$^{-1}$), thermal conductivity ($\lambda$ in W m$^{-1}$ °C$^{-1}$), and heat capacity ($c_p$ in N mm$^{-2}$ °C$^{-1}$) properties have been used in FE simulations as given in Table 3.

One of the most important inputs to the FE simulation of the chip formation process is flow stress curves at different strain, strain rate and temperature generally obtained from the material constitutive behavior model. In the literature, the material constitutive behavior of the IN718 nickel-based alloy is often represented with the Johnson–Cook (JC) model due to the model's general availability in FEM software.

DeMange et al. [20] have studied the effect of heat treatment on the room temperature quasi-static and high strain rate compression behavior of IN718 under annealed and aged conditions. The testing strain rate range for the annealed material was 1796–3506 s$^{-1}$, while it was 1681–4581 s$^{-1}$ for the aged material. The strain hardening behavior of the material was significantly greater at the annealed condition. Flow stress curves of the annealed material exhibited strong strain hardening at all strains, but curves of the aged material showed sharp softening effect around a strain value of 0.1 and remained constant after strain value of 0.25. Pereira and Lerch [12] referred to that data and suggested a set of JC model parameters

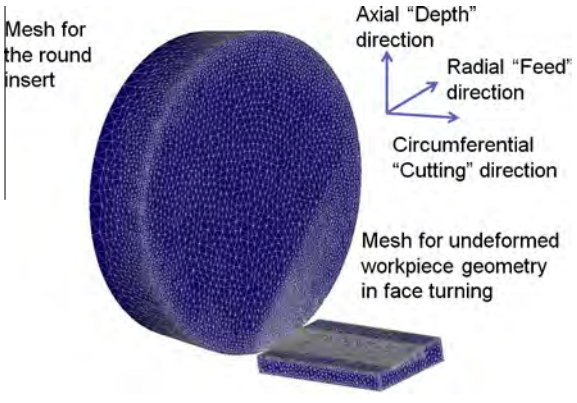


**Fig. 7.** 3-D FE model for machining [10].

**Table 3**
Properties of IN718 work and cemented tungsten carbide (WC/Co) tool material.

| | IN718 | WC/Co |
|---|---|---|
| $E\ (T)$ | $-74.35 \cdot T + 214790$ | $5.6 \times 10^5$ |
| $\alpha\ (T)$ | $10^{-5} \cdot e^{0.0004 \cdot T}$ | $4.7 \times 10^{-6}$ |
| $\lambda\ (T)$ | $11.367 \cdot e^{0.0009 \cdot T}$ | 55 |
| $c_p\ (T)$ | $418.63 \cdot e^{0.0433 \cdot T}$ | $0.0005 \cdot T + 2.07$ |

without considering thermal softening effects. The Johnson–Cook material model parameters later suggested for IN718 did not show any strain softening effect at elevated strain rates and temperatures.

Sievert et al. [15] utilized the Johnson–Cook constitutive model to simulate high speed machining of IN718 nickel-based alloy. In their study, the JC parameters for IN718 nickel-based alloy ($A$ = 450 MPa, $B$ = 1798 MPa, $C$ = 0.0134, $n$ = 0.6522) were referred to Olschewski et al. [21]. In their work, they have also provided a ductile damage model. However, it is interesting to note that these parameters are very close to those suggested by Pereira and Lerch [12] and they are a combination of annealed ($A$ and $B$) and aged ($C$ and $n$) material conditions. Mitrofanov et al. [22] suggested a new set of the JC model parameters for IN718, namely $A$ = 1241 MPa, $B$ = 622 MPa, $C$ = 0.0134, $n$ = 0.6522. Where parameters $A$ and $B$ were calculated from quasi-static material property data and rate sensitivity, $C$, and strain hardening, $n$, parameters were adopted from Pereira and Lerch [12]. Uhlmann et al. [16] also utilized the JC material model to simulate cutting of IN718 and used model parameters proposed by Sievert et al. [15] and Olschewski et al. [21]. Lorentzon et al. [8] used model parameters $A$, $B$, $C$, $n$ from Mitrofanov et al. [22] and $m$ = 1.3 from Sievert et al. [15] and Olschewski et al. [21]. The JC material model parameters reported in the literature is summarized in Table 4. The melting temperature for IN718 is reported as $T_m$ = 1297 °C in those studies.

Since a precipitation hardened IN718 nickel-based alloy workpiece material is considered in this study, the JC material constitutive model is modified to include flow softening as proposed in [18]. Therefore, the original JC model has been modified for temperature-dependent flow (strain) softening effect in addition to strain and strain rate hardening and thermal softening modified as shown in Eq. (1).

$$\sigma = \left[A + B\varepsilon^n\left(\frac{1}{exp(\varepsilon^a)}\right)\right]\left[1 + Cln\frac{\dot{\varepsilon}}{\dot{\varepsilon}_0}\right]\left[1 - \left(\frac{T - T_0}{T_m - T_0}\right)^m\right]\left[D + (1 - D)\left[tanh\left(\frac{1}{(\varepsilon + p)^r}\right)\right]^s\right] \quad (1)$$

where $D = 1 - \left(\frac{T}{T_m}\right)^d$, $p = \left(\frac{T}{T_m}\right)^b$, $\sigma$ is flow stress, $\varepsilon$ is true strain, $\dot{\varepsilon}$ is true strain rate, $\varepsilon_0$ is reference true strain, and $T$, $T_m$, $T_0$ are work, material melting and ambient temperatures respectively. In this model, the influence of strain, strain rate, temperature and temperature-dependent flow (strain) softening on the flow stress is defined by four multiplicative terms.

The difference between the present study and the study by Özel and Ulutan [11] is that the modified material model parameters for temperature-dependent flow softening behavior of IN718 nickel-based alloy were identified in a procedure by changing the model parameters until FE simulation predictions matched with the measured forces.

The contact at the tool-chip interface is modeled by using a hybrid friction model including the shear friction law and Coulomb friction combined. In the shear friction law, frictional stress ($\tau$) is proportional to effective stress ($\bar{\sigma}$) with a shear friction factor ($m_f$) as in $\tau = m_f \frac{\bar{\sigma}}{\sqrt{3}}$ In the Coulomb friction law, the frictional stress is proportional to the normal stress ($\sigma_n$) with a friction coefficient ($\mu$) as in $\tau = \mu\sigma_n$. A constant Coulomb friction coefficient of $\mu$ = 0.5 is used in all simulations since it represents sliding contact condition between WC tool and IN718 work material. However, the shear friction factor in tool-chip interface is not known. For investigation purposes, the shear friction factor was varied from $m_f$ = 0.6 up to $m_f$ = 0.9 in these FE simulations. Therefore, FE simulation models with different modified material model and friction parameters have been evaluated as given in Tables 5 and 6. The influence of flow stress model parameters and shear friction factor on FE simulation based predictions in predicted forces and stress profiles have been explored.

Force comparison is available for both different cutting speeds and feeds. In general, simulated forces in circumferential (cutting) direction ($F_c$) are usually in agreement with experimental forces whereas simulated axial ($F_p$) and radial ($F_f$) forces are lower than the experimental ones. In addition, it should be noted that experimental axial forces ($F_p$) are higher than

**Table 4**
The JC constitutive model parameters used for IN718 nickel alloy.

| Reference | $A$ (MPa) | $B$ (MPa) | $C$ (–) | $n$ (–) | $m$ (–) | $\dot{\varepsilon}_0$ ($s^{-1}$) | Heat treatment |
|---|---|---|---|---|---|---|---|
| Pereira and Lerch [12] | 450 | 1798 | 0.0312 | 0.9143 | – | 1.0 | Annealed |
| Pereira and Lerch [12] | 1350 | 1139 | 0.0134 | 0.6522 | – | 1.0 | Aged |
| Uhlmann et al. [16] | 450 | 1700 | 0.017 | 0.65 | 1.3 | 0.001 | Annealed |
| Sievert et al. [15] | | | | | | | |
| Olschewski et al. [21] | | | | | | | |
| Mitrofanov et al. [22] | 1241 | 622 | 0.0134 | 0.6522 | – | 1.0 | Aged |
| Lorentzon et al. [8] | 1241 | 622 | 0.0134 | 0.6522 | 1.3 | 1.0 | Aged |

**Table 5**
Comparison of simulation force predictions with experiments by using various material model parameters and shear friction factors at the high feed rate ($f$ = 0.25 mm rev$^{-1}$) cutting condition.

| Modified material model and friction parameters ($A$ = 1300 MPa, $n$ = 0.6522, $C$ = 0.0134, $m$ = 1.3, $T_m$ = 1297 °C, $\mu$ = 0.5) | | | | | | | Measured forces $v_c$ = 30 m min$^{-1}$ $f$ = 0.25 mm rev$^{-1}$, $a_p$ = 0.15 mm | | | Measured forces $v_c$ = 70 m min$^{-1}$ $f$ = 0.25 mm rev$^{-1}$, $a_p$ = 0.15 mm | | |
|---|---|---|---|---|---|---|---|---|---|---|---|---|
| | | | | | | | $F_c$ [N] 207 | $F_f$ [N] 42 | $F_p$[N] 259 | $F_c$ [N] 198 | $F_f$ [N] 44 | $F_p$ [N] 277 |
| | | | | | | | Simulated forces $v_c$ = 30 m·min$^{-1}$ | | | Simulated forces $v_c$ = 70 m·min$^{-1}$ | | |
| $B$ | $a$ | $d$ | $b$ | $r$ | $s$ | $m_f$ | $F_c$ ± std Error% | $F_f$ ± std Error% | $F_p$ ± std Error% | $F_c$ ± std Error% | $F_f$ ± std Error% | $F_p$ ± std Error% |
| 800 | 50 | 0.45 | 0.1 | 0.2 | −0.5 | 0.9 | 202 ± 9 3% | 22 ± 1 49% | 177 ± 7 32% | 192 ± 4 3% | 21 ± 1 48% | 177 ± 5 36% |
| 800 | 50 | 0.45 | 0.1 | 0.2 | −0.5 | 0.6 | 189 ± 8 9% | 21 ± 1 51% | 172 ± 7 34% | 181 ± 6 9% | 21 ± 1 50% | 173 ± 6 38% |
| 1100 | 50 | 0.45 | 0.1 | 0.2 | −0.5 | 0.9 | 207 ± 11 <1% | 23 ± 1 46% | 186 ± 7 28% | 198 ± 4 <1% | 23 ± 1 45% | 187 ± 7 32% |
| 1100 | 50 | 0.45 | 0.1 | 0.2 | −0.5 | 0.6 | 196 ± 13 5% | 22 ± 1 48% | 183 ± 10 29% | 185 ± 5 7% | 22 ± 1 47% | 183 ± 7 34% |

**Table 6**
Comparison of simulation force predictions with experiments by using various material model parameters and shear friction factors at the low feed rate ($f$ = 0.15 mm rev$^{-1}$) cutting condition.

| Modified material model and friction parameters ($A$ = 1300 MPa, $n$ = 0.6522, $C$ = 0.0134, $m$ = 1.3, $T_m$ = 1297 °C, μ = 0.5) | | | | | | | Measured forces $v_c$ = 30 m min$^{-1}$ $f$ = 0.15 mm rev$^{-1}$, $a_p$ = 0.15 mm | | | Measured forces $v_c$ = 70 m min$^{-1}$ $f$ = 0.15 mm rev$^{-1}$, $a_p$ = 0.15 mm | | |
|---|---|---|---|---|---|---|---|---|---|---|---|---|
| | | | | | | | $F_c$ (N) 160 | $F_f$ (N) 42 | $F_p$ (N) 226 | $F_c$ (N) 148 | $F_f$ (N) 44 | $F_p$ (N) 266 |
| | | | | | | | Simulated forces $v_c$ = 30 m min$^{-1}$ | | | Simulated forces $v_c$ = 70 m min$^{-1}$ | | |
| $B$ | $a$ | $d$ | $b$ | $r$ | $s$ | $m_f$ | $F_c$ ± std Error% | $F_f$ ± std Error% | $F_p$ ± std Error% | $F_c$ ± std Error% | $F_f$ ± std Error% | $F_p$ ± std Error% |
| 800 | 50 | 0.45 | 0.1 | 0.2 | −0.5 | 0.9 | 151 ± 8 6% | 20 ± 1 53% | 158 ± 7 30% | 145 ± 3 2% | 20 ± 1 55% | 160 ± 5 40% |
| 800 | 50 | 0.45 | 0.1 | 0.2 | −0.5 | 0.6 | 143 ± 6 11% | 20 ± 1 53% | 158 ± 7 30% | 137 ± 3 7% | 20 ± 1 55% | 160 ± 6 40% |
| 1100 | 50 | 0.45 | 0.1 | 0.2 | −0.5 | 0.9 | 158 ± 4 1% | 21 ± 1 50% | 168 ± 5 26% | 148 ± 4 <1% | 21 ± 1 53% | 169 ± 6 37% |
| 1100 | 50 | 0.45 | 0.1 | 0.2 | −0.5 | 0.6 | 149 ± 5 7% | 21 ± 1 50% | 169 ± 7 25% | 143 ± 34 3% | 21 ± 4 52% | 171 ± 35 36% |

cutting forces ($F_c$) which is an opposite trend than conventional turning processes. This may be due to a very low depth of cut ($a_p$ = 0.15 mm) taken by a tool insert with a relatively very large nose radius ($r_\varepsilon$ = 4 mm).

The parameters of the modified flow stress model highly influence FE simulation predictions. Therefore, a procedure was adopted to identify the effects of each parameter and hence identify the best model parameter set until a reasonable match (about 1% error) in simulated and measured cutting forces is achieved. This procedure was highlighted with some selected examples in Tables 5 and 6. It was concluded that flow stress model parameters of $A$ = 1300, $B$ = 1100, $n$ = 0.6522, $C$ = 0.0134, $m$ = 1.3, $T_m$ = 1297 °C, $a$ = 50, $d$ = 0.45, $b$ = 0.1, $p$ = 0, $r$ = 0.2, $s$ = −0.5 provided the best match of the predicted cutting forces with the measured ones at both cutting speeds of $v_c$ = 30 and 70 m min$^{-1}$ and feeds of $f$ = 0.15 and 0.25 mm rev$^{-1}$. Moreover, shear friction factor was varied and force predictions were further improved by using a shear friction factor of $m_f$ = 0.9.

Flow stress curves of the modified JC material model with the identified model parameters at different temperatures and strain rates are compared with the JC models reported by Pereira and Lerch [12] and Lorentzon et al. [8] in Fig. 8. These flow stress curves depict strain softening behavior of IN178 material especially around a strain value of $\varepsilon$ = 1 mm mm$^{-1}$, and thermal softening behavior at elevated temperatures. Furthermore, it can be noticed that flow stress curves at high temperatures are not much affected by increasing strain rate.

In addition, distributions of effective (von Mises) strain, effective (von Mises) stress, and temperature in the chip and on the machined workpiece surface are given in Figs. 9–11, using the material model parameters that provided the best match between experimental and simulated forces at all cutting conditions. The effective strain distributions given in Fig. 9 reveal very similar results. Concerning the effective stress distributions given in Fig. 10, it is possible to observe that in the tool-chip contact area effective stress values are practically the same.

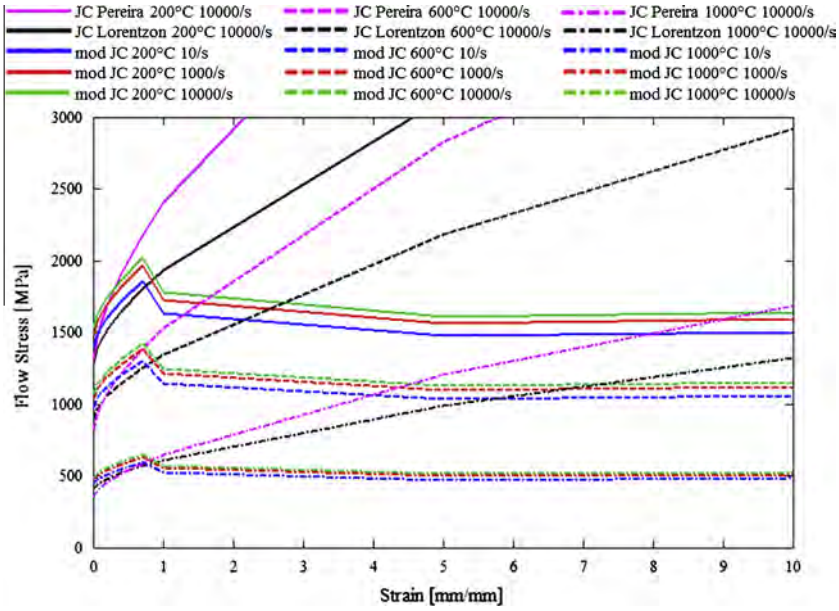


**Fig. 8.** Flow stress curves of the modified JC material model as compared with the JC model.

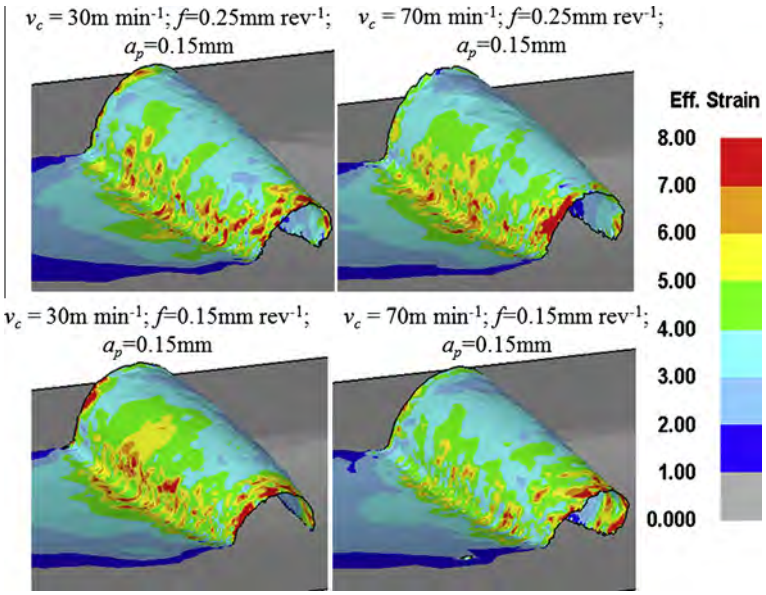


**Fig. 9.** Effective (von Mises) strain distributions in the chip obtained from 3-D FE simulations at a cutting length of 1.2 mm.

At the higher cutting speed, the cutting temperatures given in Fig. 11 are found higher due to higher plastic deformation rate and higher heat generation. In case of the lower cutting speed, the temperature distribution in the chip is higher even when a lower feed rate is employed. This localized high heat build-up is probably due to a combination of poor thermal conductivity of IN718 nickel-based alloy, and a small tool-chip contact area.

## 5. Comparison of residual stress predictions with measurements

A detailed comparison of experimentally measured stress profiles on machining surfaces and predicted residual stresses from the results of the 3-D FE simulations is also given in Figs. 12–15. In these figures, experimentally measured residual stress profiles are represented with dashed lines together with the measurement uncertainty which is represented with a vertical bar at each measurement depth.

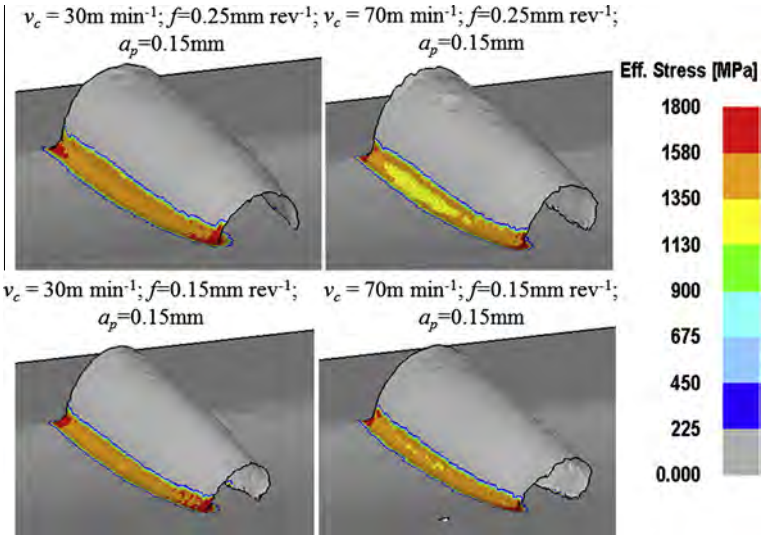


**Fig. 10.** Effective (von Mises) stress distributions in the chip obtained from 3-D FE simulations at a cutting length of 1.2 mm.

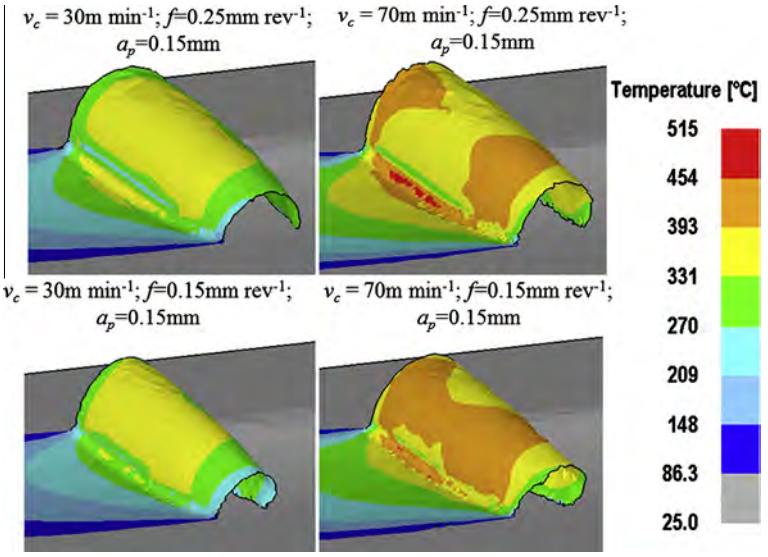


**Fig. 11.** Temperature distributions in the chip obtained from 3-D FE simulations at a cutting length of 1.2 mm.

In FE simulations, stress profiles into the depth of material were obtained from several locations on the machined surface and average stress values and standard deviations were calculated. In these figures, solid lines represent average stress values and vertical bars with round ends represent standard deviations at each depth level. These variations in predictions are due to fluctuations in predicted machining induced stress fields and their average values are presented together with their standard deviations. It should be noted that the stress profiles predicted from FE simulations (marked as simulated) have larger variations than the measurements. These are mainly caused by the remeshing generated variations in the contact between the tool and the workpiece and to a certain degree by the chip formation. Experimentally measured residual stress profiles are generally hook-shaped; beginning with a high tensile stress at the surface and reaching a high compressive stress value after a decline at around 0.02–0.03 mm depth and then quickly recovering to reach near-zero values into the depth of material at around 0.25 mm depth. Predicted stress profiles are also hook-shaped and in agreement with experiments predicting the peak tensile stress in general. Predicted peak compressive stresses often occur at a deeper level into the material and remain significant in a depth range (around 0.03–0.06 mm). Existence of peak tensile stress on the surface is mainly due to thermal strain associated with cutting whereas peak compressive stress into depth of material is caused by plastic deformations. Hence, the degree of thermal–mechanical work is decisive of these stresses. Therefore, in case of the higher cutting speed, more heat is generated but the increase in the severity of plastic deformation into depth of material is not as much as

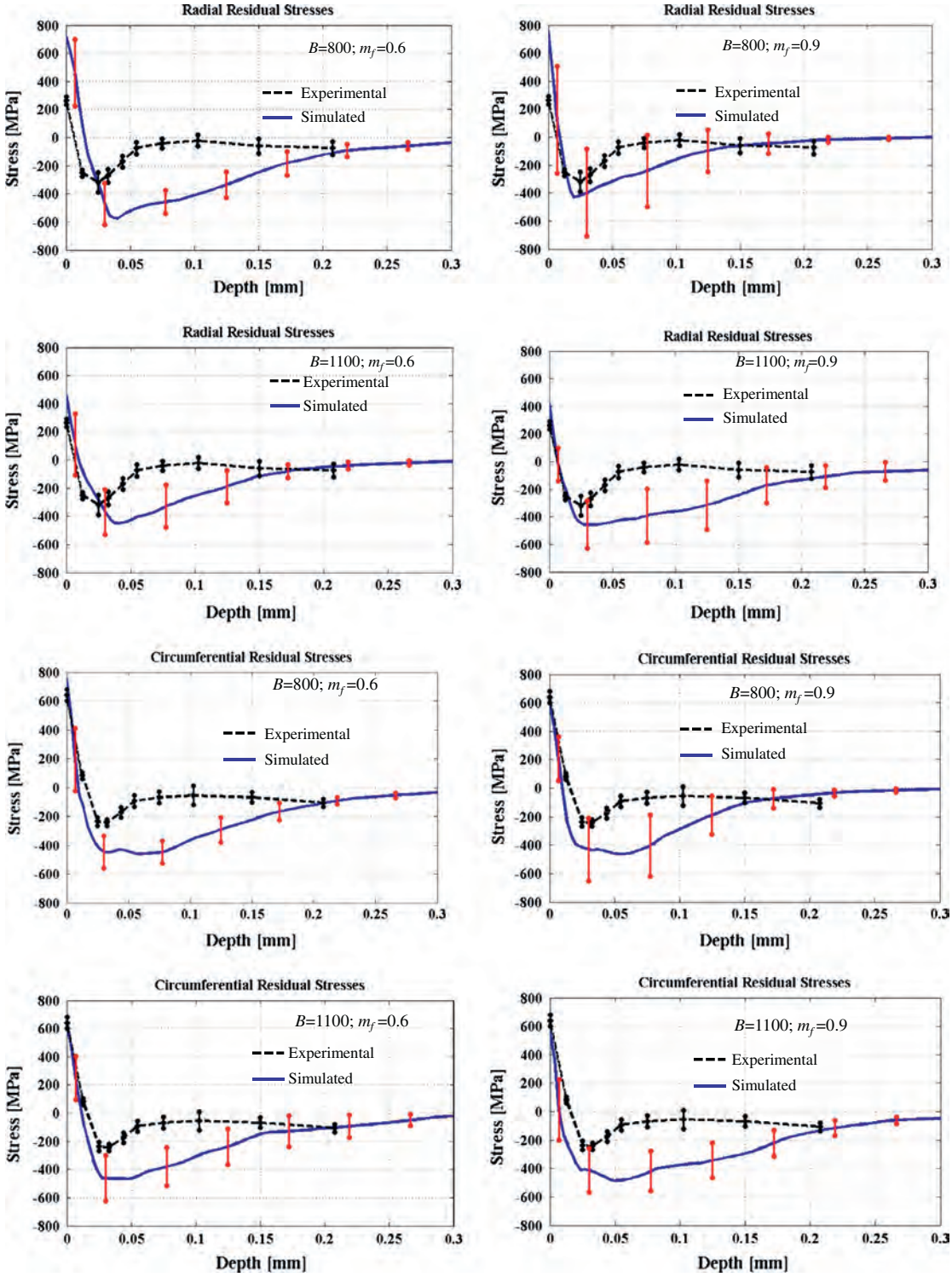


**Fig. 12.** Comparison of measured and simulated residual stress profiles and effect of material model parameter and shear friction factor ($v_c$ = 30 m min$^{-1}$, $f$ = 0.15 mm rev$^{-1}$, $a_p$ = 0.15 mm).

the increase of heat generated. In case of the lower feed rate, depth of plastic deformations increases as well as the magnitude of compressive residual stress. However it should be noted that the influence of feed rate is not so significant since the feed rate levels experimented are close to each other and tool nose radius is very large when compared to depth of cut.

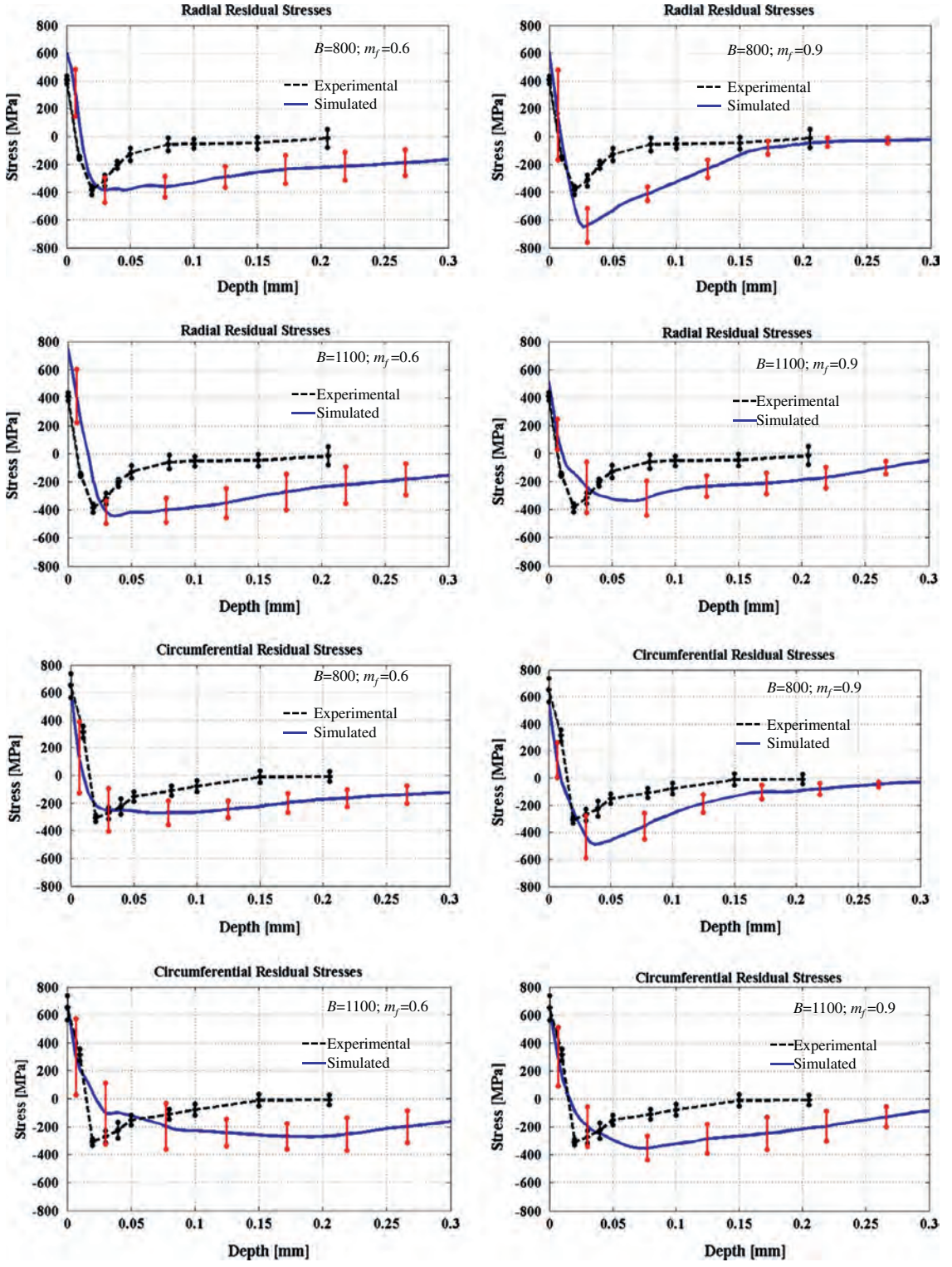


**Fig. 13.** Comparison of measured and simulated residual stress profiles and effect of material model parameter and shear friction factor ($v_c$ = 30 m min$^{-1}$, $f$ = 0.25 mm rev$^{-1}$, $a_p$ = 0.15 mm).

Similar trends in machining induced residual stress profiles have been observed in machining of IN718 nickel-based alloy material [1].

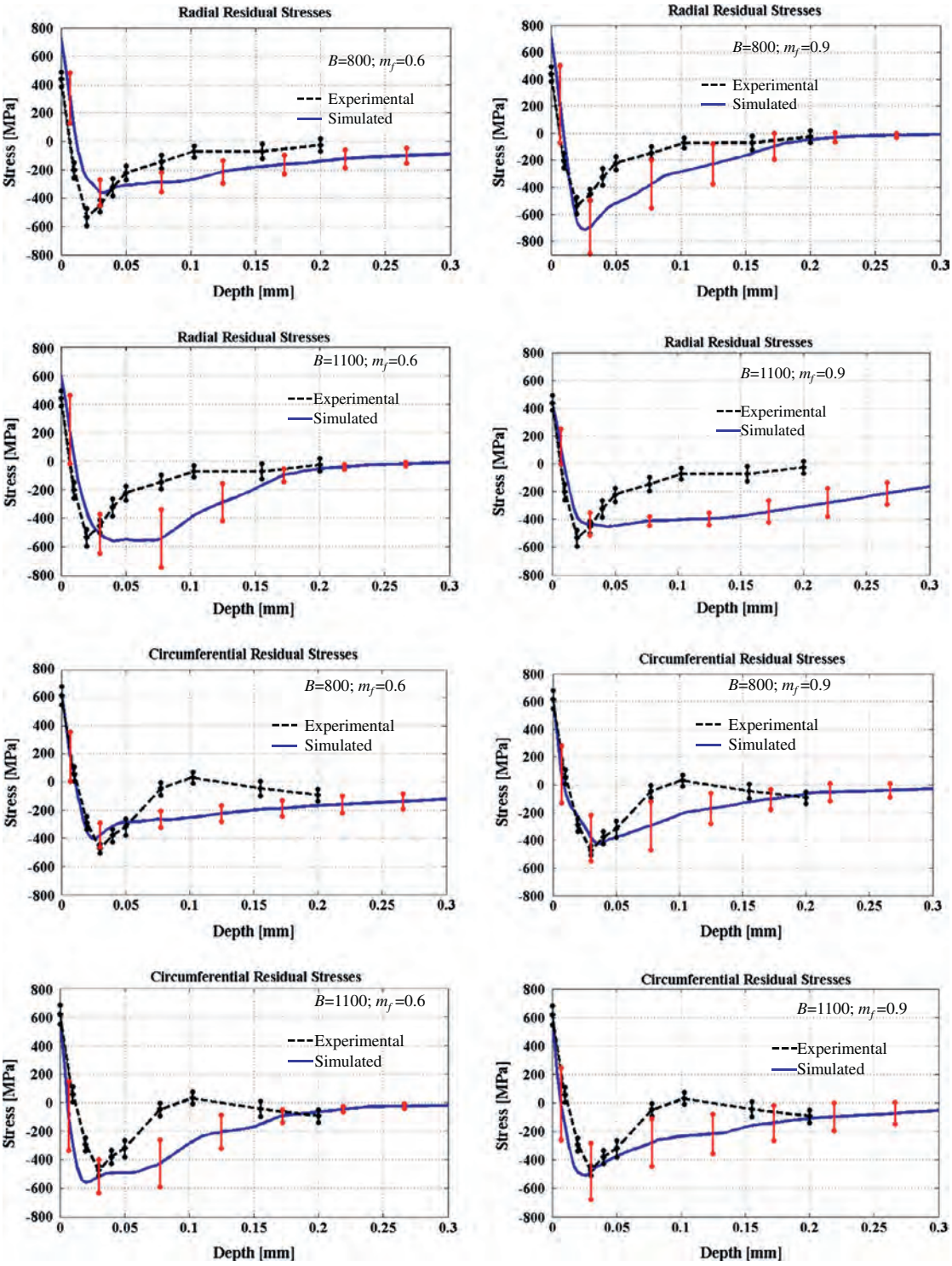


**Fig. 14.** Comparison of measured and simulated residual stress profiles and effect of material model parameter and shear friction factor ($v_c$ = 70 m min$^{-1}$, $f$ = 0.15 mm rev$^{-1}$, $a_p$ = 0.15 mm).

In general, predicted stress profiles were found to be in good agreement with experimental measurements when modified material model and friction parameters are properly identified and utilized in 3-D FE simulations. The effects of modified flow stress parameters and the shear friction factor were apparent as presented in Figs. 12–15. These results depict the influence of friction model and flow stress parameters on the predicted machining induced stress profiles. Especially, comparison

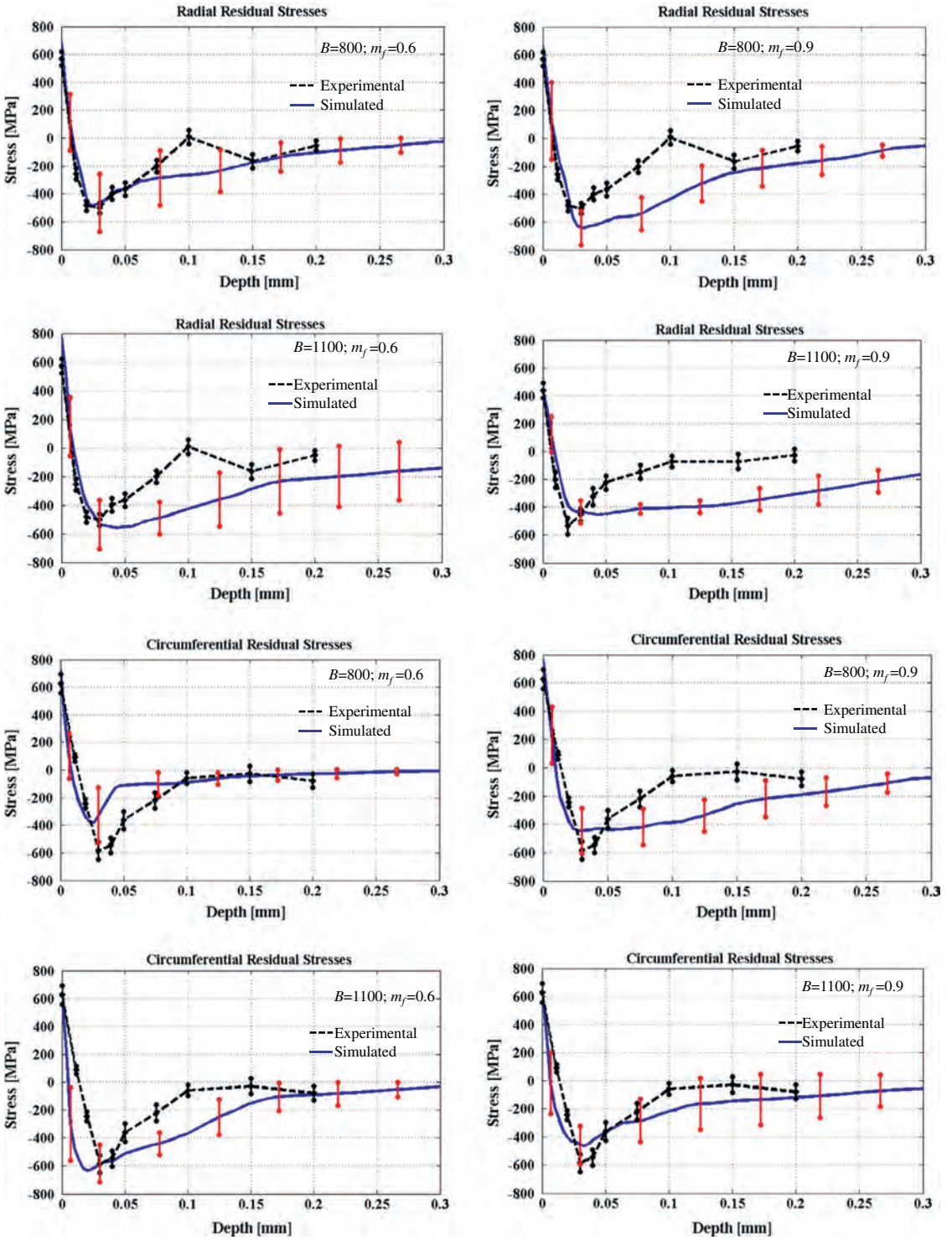


**Fig. 15.** Comparison of measured and simulated residual stress profiles and effect of material model parameter and shear friction factor ($v_c$ = 70 m min$^{-1}$, $f$ = 0.25 mm rev$^{-1}$, $a_p$ = 0.15 mm).

of predicted and measured residual stress profiles reveals that the agreement is better at the lower cutting speed of $v_c$ = 30 m min$^{-1}$ due to lower contribution of thermal strain. However, predicted stresses on the surface were more tensile and greater than the measured ones due to the higher thermal strain involved in machining induced stress profiles in FE simulations. In addition, predicted compressive peak stresses were greater than the measured ones in radial direction

indicating that the plastic deformation mechanism was more dominant than thermal strain generation during FE simulations. It was concluded that flow stress model parameters of $A = 1300$ MPa, $B = 1100$ MPa, $n = 0.6522$, $C = 0.0134$, $m = 1.3$, $T_m = 1297$ °C, $a = 50$, $d = 0.45$, $b = 0.1$, $p = 0$, $r = 0.2$, and $s = -0.5$ have provided the best match of the predicted cutting forces with the measured ones at both cutting speeds of $v_c = 30$ and $70\ \mathrm{m\ min^{-1}}$ and feeds of $f = 0.15$ and $0.25\ \mathrm{mm\ rev^{-1}}$. In addition, it was observed that same material model parameter set has provided the best match in measured and simulated residual stress profiles.

## 6. Conclusions

In this study, residual stress measurement techniques and machining induced stress predictions using 3-D FE-based simulations have been studied. The main methods of measuring residual stresses including diffraction techniques have been critically reviewed. It appears that measurements obtained with diffraction methods for residual stresses are more accurate. Then, predictions of machining induced stresses using 3-D FE simulations and comparison of experimentally measured residual stresses for machining of IN718 have been investigated. The influence of friction and material flow stress on the machining induced stress profiles has been also explored. Flow stress material model parameters and their effects for predicting stresses in IN718 have been identified and presented. The main result of this study indicates that stress predictions have significant variations and can be better represented by using average and standard deviations. Specific conclusions can be given as follow:

- In general, the predicted residual stress profiles and the experimental residual stress profiles have the same hook shape, being more attractive on the surface, reaching a compressive peak into the depth and recovering to near zero values at higher depths.
- The tractive residual stresses reached on the surface are higher in the circumferential direction than in the radial direction, and also the compressive peak is higher in circumferential direction.
- The influence of feed rate is very low due to the cutting tool geometry employed in this study, and also its influence is more considerable in radial direction.
- Besides, when increasing cutting speed both surface residual stress and maximum compressive peak stress are higher in the range of cutting parameters tested in this research work.
- The depth of machining affected layer is found higher in the FE simulation predictions.
- The experimental residual stress results and the simulated residual stresses agree better at the lower cutting speed condition.

## Acknowledgements

The authors from Rutgers University acknowledge the financial support provided by the National Science Foundation (Grant Number CMMI-1130780), and support for DEFORM software by SFTC, Ohio, USA.

The authors from Mondragon University thank the Basque and Spanish Governments for the financial support given to the projects PROFUTURE I (code IE10-271) and PROFUTURE II (code IE11-308) and METINCOX (DPI2009-14286-C02-0 and PI-2010-11).

## References

[1] R.M. Arunachalam, M.A. Mannan, A.C. Spowage, Surface integrity when machining age hardened Inconel 718 with coated carbide cutting tools, Int. J. Mach. Tools Manuf. 44 (2004) 1481–1491.
[2] M. Belassel, J. Pineault, M.E. Brauss, Comparison and evaluation of residual stress measurement techniques, a technical and economical study, Proc. SEM Ann. Conf. Expos. Experiment. Appl. Mech. 2 (2011) 756–762.
[3] A. Benediktovich, H. Guerault, I. Feranchuk, V. Uglov, A. Ulyanenkov, Influence of surface roughness on evaluation of stress gradients in coatings, Mater. Sci. Forum 681 (2011) 121–126.
[4] I.S. Jawahir, E. Brinksmeier, R. M'Saoubi, D.K. Aspinwall, J.C. Outeiro, D. Meyer, D. Umbrello, A.D. Jayal, Surface integrity in material removal processes: recent advances, CIRP Ann. – Manuf. Technol. 60 (2011) 603–626.
[5] A. Kortabarria, A. Madariaga, E. Fernandez, J.A. Esnaola, P.J. Arrazola, A comparative study of residual stress profiles on Inconel 718 induced by dry face turning, Proc. Eng. 19 (2011) 228–234.
[6] W. Li, P.J. Withers, M. Preuss, J. Shackleton, P. Andrews, Depth and lateral variation of machining-induced residual stress for a nickel base superalloy, Mater. Sci. Forum 681 (2011) 332–339.
[7] J.D. Lord, P.V. Grant, A.T. Fry, F.A. Kandil, A UK residual stress intercomparison exercise – development of measurement good practice for the XRD and hole drilling techniques, Mater. Sci. Forum 404–407 (2002) 567–572.
[8] J. Lorentzon, N. Järvstråt, B.L. Josefson, Modelling of chip formation of alloy 718, J. Mater. Process. Technol. 209 (2009) 4645–4653.
[9] J.C. Outeiro, J.C. Pina, R. M'Saoubi, F. Pusavec, I.S. Jawahir, Analysis of residual stresses induced by dry turning of difficult-to-machine materials, CIRP Ann. – Manuf. Technol. 57 (1) (2008) 77–80.
[10] T. Özel, I. Llanos, J. Soriano, P.J. Arrazola, 3D finite element modelling of chip formation process for machining Inconel 718: comparison of FE software predictions, Mach. Sci. Technol. 15 (1) (2011) 21–46.
[11] T. Özel, D. Ulutan, Prediction of machining induced residual stresses in turning of titanium and nickel based alloys with experiments and finite element simulations, CIRP Ann. – Manuf. Technol. 61 (1) (2012) 547–550.
[12] J.M. Pereira, B.A. Lerch, Effects of heat treatment on the ballistic impact properties of Inconel 718 for jet engine fan containment applications, Int. J. Impact Eng. 25 (2001) 715–733.

[13] C.O. Ruud, P.S. DiMascio, J.J. Yavelak, Comparison of three residual stress measurement methods on a mild steel bar, Exp. Mech. 25 (4) (1985) 338–343.
[14] R. M'Saoubi, J.C. Outeiro, H. Chandrasekaran, O.W. Dillon, I.S. Jawahir, A review of surface integrity in machining and its impact on functional performance and life of machined products, Int. J. Sust. Manuf. 1 (2008) 203–236.
[15] R. Sievert, H.D. Noack, A. Hamann, P. Loewe, K.N. Singh, G. Kuenecke, R. Clos, U. Schreppel, P. Veit, E. Uhlmann, R. Zettier, Simulation der spansegmentierung beim hochgeschwindigkeits-zerspanned unter berücksichtigung duktiler schädigung, Tech. Mechan. 23 (2–4) (2003) 216–233.
[16] E. Uhlmann, M. Graf von der Schulenburg, R. Zettier, Finite element modeling and cutting simulation of Inconel 718, Ann. CIRP 56 (1) (2007) 61–64.
[17] D. Ulutan, T. Özel, Machining induced surface integrity in titanium and nickel alloys: a review, Int. J. Mach. Tools Manuf. 51 (2011) 250–280.
[18] D. Ulutan, M. Sima, T. Özel, Prediction of machining induced surface integrity using elastic–viscoplastic simulations and temperature-dependent flow softening material models in titanium and nickel-based alloys, Adv. Mater. Res. 223 (2011) 401–410.
[19] D. Walker, Residual stress measurement techniques, Adv. Mater. Process. 159 (8) (2001) 30–33.
[20] J.J. DeMange, V. Prakash, J.M. Pereira, Effects of material microstructure on blunt projectile penetration of a nickel-based super alloy, Int. J. Impact Eng. 36 (2009) 1027–1043.
[21] J. Olschewski, A. Hamann, M. Bendig, et al., Werkstoffmechanik einer Nickelbasislegierung beim Hochgeschwindigkeitsspanen- Werkstoffverhalten und Modellierung, Teil II, Report BAM-V.2 01/3, Bundesanstalt für Materialforschung und prüfung (BAM), Berlin, 2001.
[22] A.V. Mitrofanov, V.I. Babitsky, V.V. Silberschmidt, Thermomechanical finite element simulations of ultrasonically assisted turning, Comput. Mater. Sci. 32 (3–4) (2005) 463–471.